Preconditioning the coupled heart and torso bidomain model with an almost linear complexity

Charles Pierre

PRECONDITIONING THE COUPLED HEART AND TORSO BIDOMAIN MODEL WITH AN ALMOST LINEAR COMPLEXITY

CHARLES PIERRE

Abstract. The bidomain model is widely used in electro-cardiology to simulate spreading of excitation in the myocardium and electrocardiograms. It reads a system of two parabolic reaction diffusion equations coupled with an ODE system. Its discretization displays an ill-conditioned system matrix to be inverted at each time step: simulation based on the bidomain model therefore are associated with high computational costs. In this paper we propose a preconditioning for the bidomain model in an extended framework including a coupling with the surrounding tissues (the torso). The preconditioning is based on a formulation of the discrete problem that is shown to be symmetric positive. A block LU decomposition of the system together with a heuristic approximation (referred to as the monodomain model) are the key ingredients for the preconditioning definition. Numerical results are provided for two test cases: a 2D realistic one (based on a segmented heart medical image geometry) and a 3D academical one. The analysis of the resulting computational cost (both in terms of CPU time and of iteration number) show an almost linear complexity, i.e. of type $n \log^{\alpha}(n)$.

1. Introduction

The bidomain model [28, 16, 1, 10, 29] is up to now the most physiologically founded model to describe the heart electrical activity. The bidomain model is here considered in an extended version referred to as the *coupled heart and torso bidomain model*. It includes a coupling of the cardiac electrical activity with the surrounding tissue electrical activity, allowing in particular electrocardiogram simulations.

The bidomain model mathematical formulation reads a system of two PDEs (parabolic reaction diffusion equations) describing the evolution of two potentials: the *intra-* and *extra-cellular potentials* within the myocardium. This system is coupled with a set of ODEs modelling the kinetic of ionic transfer across the cellular membranes.

The mathematical structure of the bidomain model implies that its discretization provides an ill conditioned system matrix, to be inverted at each time step. Two reasons are risen for this. The bidomain model can be formulated as a degenerate system of two coupled parabolic equations [25, 10], which degeneracy causes ill-conditioning. Another formulation of the bidomain model, reading a single scalar semi-linear parabolic equation, is studied in [4]. This formulation involves a non-local operator of second order in space, referred to as the *bidomain operator*. The bidomain operator is defined as the harmonic mean between two elliptic operators. The non locality of the bidomain operator generates high computational costs. On

Date: September 15, 2010.

Key words and phrases. Preconditioning, electro-cardiology, bidomain and monodomain models, hierarchical matrices, reaction diffusion equations, numerical simulations.

top of this structural ill-preconditioning, the physical features of the modelled phenomena (because of fast and sharp space and time variations of potential, namely potential wave fronts) necessitates to resort to fine space and time grids. Ill conditioning together with fine meshes imply very high computational costs for the bidomain model simulations that remain challenging for 3D realistic settings. For this, many efforts were devoted to the reduction of this cost, see e.g. [8, 11, 7].

The so called *monodomain model* provides a very good approximation of the bidomain model [6, 9, 21, 20]. It has been shown in [20] that a monodomain model could provide activation time mappings in complex situations with 1% of relative error as compared to the bidomain model predictions. The monodomain model reads a single unsteady reaction diffusion equation coupled with the ODE system modelling the cell membrane. It therefore provides a much more affordable way to simulate the cardiac electrical activity than the bidomain model, although lacking physiological foundations. The accuracy of this approximation can in particular greatly help in building more efficient numerical methods to solve the bidomain model [27, 19, 13].

In this paper we propose a preconditioner for the bidomain system matrix displaying an almost linear complexity, i.e. of $n \log^{\alpha}(n))$ type, with n the matrix size, partially based on the monodomain approximation heuristic. Quite general space discretizations (including classical Lagrange P^k finite element or various finite volume techniques) can be considered. For simplicity we adopted here an Euler semi-implicit time discretization but the technique generalises to more sophisticated time schemes. The preconditioning is based on the positive self adjoint formulation of the bidomain model in [4]. Once discretised, this formulation involves the inversion of one system matrix per time step that is here shown to be symmetric positive. The two following points are used to precondition the system matrix.

1- LU factorization. The system matrix displays a 2×2 block structure that can be factorised into a block-LU form.

2- Monodomain model heuristic. Among the blocks of the LU factorization, all blocks have a clear definition and do not lead to computational difficulties excepted one block. This block is shown to be symmetric positive and to be the sum of a mass matrix and of a *discrete bidomain operator* (discrete analogue of the earlier on evocated bidomain operator) that is shown to read the harmonic mean between two stiffness matrices. This block, that is not sparse, is not computed but approximated using the monodomain model approximation.

The last layer for the preconditioning is the practical definition of local preconditioners for stiffness matrices. This is done here using the hierarchical matrices theory [3, 14, 15].

In a recent paper [12], Gerardo-Giorda et al. introduced a preconditioner for the bidomain model also based on the monodomain model heuristic and on a lower block triangular approximation. The LU factorization presented here should provide more efficient algorithms than the lower bock-triangular approximation since this factorization is exact. The formulation in [12] is based on a non symmetric formulation whereas we here consider a symmetric positive system matrix. This allows to resort to more efficient iterative solvers (basically a Conjugate Gradient (CG) versus a GMRes solver). Although the global complexity might be the same, the

constants may differ implying a significant gain in term of computational cost. In earlier computations we experienced that switching from the non symmetric bidomain formulation in [2] (associated with a GMRes solver) to the positive symmetric formulation presented here (together with a CG solver) provided a speed up with factor 5-8. Eventually the positive symmetric formulation presented here naturally holds for the coupled heart and torso bidomain model whereas the preconditioner in [2] holds for an isolated heart. Our preconditioning strategy thus can be used to simulate the heart and torso coupled electrical activity for instance to recover electrocardiogram recordings.

The paper is organised as follows. The coupled heart and torso bidomain model is stated in Sec. 2., its numerical discretization follows in Sec. 3. Sec. 4 studies the mathematical properties of the discretised bidomain problem system matrix: it is here shown to be symmetric positive, its LU block factorization is then analysed. The preconditioner is defined in Sec. 5, its practical implementation analysis follows. The complexity of the preconditioned system matrix inversion is numerically studied in Sec. 6 using two test cases. The first one is a 2D realistic test case on a geometry of the heart and of the surrounding organs obtained by segmenting a medical image [22, 23] and including rotating anisotropy inside the heart. The second one is a 3D test on a simple cubic geometry (a slab of cardiac tissue).

2. Bidomain model of the heart embedded in the torso

Let us denote by Ω and H two bounded open subsets such that $H \subset \Omega \subset \mathbb{R}^d$ with $d = 2,\ 3$ and with smooth boundaries. We moreover assume that $\partial\Omega \cap \partial H = \emptyset$. Ω represents a thorax and H the region occupied by the heart (assumed fixed here). We also consider $T := \Omega - \overline{H}$ that will be referred to as the *torso*, see Fig. 1. We denote Q, Q_H and Q_T the time-space cylinder $(0,T)\times\Omega$, $(0,T)\times H$ and $(0,T)\times T$ respectively.

Two potential fields will be involved, the transmembrane potential $v :\ Q_H \mapsto \mathbb{R}$ and the potential $u :\ Q \mapsto \mathbb{R}$. When restricted to H (*resp.* to T), the potential u is referred to the extra-cellular potential (*resp.* extra cardiac potential), v is the difference of this extra-cellular potential with an intra-cellular potential not considered here.

The heart has a fibrous organization implying anisotropic electrical conductivities. The cardiac fibres rotate around the ventricle cavities, see Fig. 1. The fibres remain tangent to the cardiac boundaries. This anisotropy is taken into account by introducing in H two tensors σ_i and σ_e. Introducing the 4 conductivity parameters $g^l_{i,e}$, $g^t_{i,e}$, they read:

$$\sigma_i(x) = \mathrm{Diag}(g^l_i, g^t_i), \quad \sigma_e(x) = \mathrm{Diag}(g^l_e, g^t_e),$$

in a moving system of coordinates whose principal direction is given by the fibre orientation at point x. When written in a fixed basis, these tensors thus no longer are diagonal.

The torso region T is assumed to have an isotropic electrical conductivity. We define in T the conductivity tensor $\sigma_T(x) = k(x)Id$ where the conductivity $k : T \mapsto \mathbb{R}$ basically is piecewise constant on the different organs considered in T.

The torso model reads:

$$\begin{cases} \operatorname{div}(\sigma_T(x)\nabla u) = 0, & (t,x) \in Q_T, \\ \nabla u \cdot \mathbf{n} = 0 & \text{on} \quad \partial\Omega, \end{cases} \tag{1}$$

where $\mathbf{n}$ denotes the outward unit normal to $\partial\Omega$.

In the heart region, the bidomain model reads the three following equations in H, for $(t,x) \in Q_H$:

$$\begin{cases} \operatorname{div}((\sigma_i(x)+\sigma_e(x))\nabla u) = -\operatorname{div}(\sigma_i(x)\nabla v), \\ \chi\left(c\partial_t v + I_{ion}(v,\mathbf{w}) - I_{st}(t,x)\right) = \operatorname{div}(\sigma_i(x)\nabla(u+v)), \\ \partial_t \mathbf{w} = g(v,\mathbf{w}). \end{cases} \tag{2}$$

In line 2, c denotes the cell membrane surface capacitance, χ is the rate of cell membrane surface per unit volume, $I_{st} : Q_H \mapsto \mathbb{R}$ is the stimulation current (source term). $I_{ion}(v,\mathbf{w})$ (reaction term) denotes the surface ionic current distribution on the membrane. The gating variable $\mathbf{w} : Q_H \mapsto \mathbb{R}^p$ characterizes the state of the cell membrane, its evolution is ruled by the ODE system in line 3. The definitions of I_{ion} and of g are fixed by the chosen ionic model in Sec. 6.1.
Equations (2) are coupled with the torso model (1) with the following coupling condition:

$$\text{on} \quad \partial H : \quad \begin{cases} u_{|H} = u_{|T}\ , \quad \sigma_e(x)\nabla u_{|H}\cdot\mathbf{n} = \sigma_T(x)\nabla u_{|T}\cdot\mathbf{n}, \\ \sigma_i\nabla u_{|H}\cdot\mathbf{n} + \sigma_i\nabla v\cdot\mathbf{n} = 0. \end{cases} \tag{3}$$

where $\mathbf{n}$ denotes the outward unit normal to ∂H.

The model is closed by imposing initial conditions on v and $\mathbf{w}$,

$$v(0,x) = v_0(x), \quad \mathbf{w}(0,x) = \mathbf{w}_0(x), \quad x \in H. \tag{4}$$

Clearly, the potential field u is defined up to an additive constant. We therefore impose the normalization condition

$$\int_\Omega u(t,\cdot)dx = 0. \tag{5}$$

2.1. **Weak formulation.** We introduce the tensor $\overline{\sigma}_1$ on Ω:

$$\overline{\sigma}_1(x) = \begin{cases} \sigma_i(x)+\sigma_e(x), & x \in H \\ \sigma_T(x), & x \in T \end{cases}.$$

The weak formulation of the bidomain model (1), (2), (3) reads: $\forall \psi \in H^1(\Omega)$, $\forall \phi \in H^1(H)$,

$$\begin{cases} \displaystyle\int_\Omega \overline{\sigma}_1\nabla u\cdot\nabla\psi dx + \int_H \sigma_i\nabla v\cdot\nabla\psi dx = 0, \\ \displaystyle\chi c\partial_t\int_H v\phi dx + \chi\int_H (I_{ion}(v,\mathbf{w}) - I_{st}(x,t))\phi dx = -\int_H \sigma_i\nabla(u+v)\cdot\nabla\phi dx, \end{cases} \tag{6}$$

The first line in (6) is obtained by multiplying (1) and the first equation in (2) by a test function $\psi \in H^1(\Omega)$, by integrating on Ω and by using the coupling conditions (3) and the boundary condition on $\partial\Omega$ in (1). The second line in (6) is obtained by multiplying the second equation in (2) by a test function $\phi \in H^1(H)$, by integrating on H together with (3).

2.2. **Case of an isolated heart.** We here address the particular case where the heart is considered as isolated from the surrounding tissues. In this case we have $H = \Omega$ and $T = \emptyset$. Equations (2) only are considered and the coupling conditions (3) are replaced by zero flux boundary conditions on ∂H for v and u.

3. Implementation

For more simplicity, temporal discretization is fixed to a semi implicit Euler scheme: implicit for the diffusion and explicit on the reaction. The implementation presented here as well as the associated preconditioner presented in the following section could however be generalized to more sophisticated time discretization as discussed in remark 2.

The implementation strategy is similar for various space discretizations including P^k Lagrange finite elements or finite volume scheme such as the CVFE scheme (Control Volume Finite Element, see eg [5]) that will be used here to compute some the numerical results or such as the DDFV scheme in [2]. Assumptions $(H1)$ and $(H2)$ on the space discretization are detailed in Sec. 3.1 whereas the numerical scheme itself is presented in Sec. 3.2.

3.1. **Settings.** Let us consider a mesh $\mathfrak{M}$ of Ω and a mesh $\mathfrak{M}_H$ of the cardiac region H: we assume that $\mathfrak{M}_H$ is a sub mesh of $\mathfrak{M}$, that is to say that all elements (or cells or control volumes) of $\mathfrak{M}_H$ also are elements of $\mathfrak{M}$.

Relatively to the considered space discretization, let us denote by $\mathbb{R}^{\mathfrak{M}}$, $\mathbb{R}^{\mathfrak{M}_H}$ the set of discrete functions attached to these two meshes. Their dimensions are respectively denoted N and N_H. A "*natural*" basis usually is provided for $\mathbb{R}^{\mathfrak{M}}$ and $\mathbb{R}^{\mathfrak{M}_H}$, respectively denoted $(U_i)_{1\leq i\leq N}$ and $(U_i^H)_{1\leq i\leq N_H}$. In the case of P^k finite element methods, these functions simply are the standard P^k Lagrange basis functions. Considering these basis induces an isomorphism between $\mathbb{R}^{\mathfrak{M}}$ and $\mathbb{R}^N$ and between $\mathbb{R}^{\mathfrak{M}_H}$ and $\mathbb{R}^{N_H}$. A discrete function $U = \sum_{i=1}^N c_i U_i$ will be considered either as a real function or as the real vectors $(c_i)_{i\leq 1\leq N}$. Using these identifications, the canonical Euclidian structures on $\mathbb{R}^N$ and $\mathbb{R}^{N_H}$ extend to $\mathbb{R}^{\mathfrak{M}}$ and $\mathbb{R}^{\mathfrak{M}_H}$. We denote by $(\cdot,\cdot)_{\mathfrak{M}}$ and $(\cdot,\cdot)_{\mathfrak{M}_H}$ the associated scalar products.

We make the following first assumption on the space discretization method:

- $(H1)$ for all i, $1 \leq i \leq N_H$: $U_{i|H} = U_i^H$ (where $U_{i|H}$ denotes the restriction of the function U_i to H).

In the case of the P^k finite element methods, this first assumption is true modulo a reordering of the basis function $(U_i)_{1\leq i\leq N}$. Assumption $(H1)$ allows us to define the restriction operation:

$$\Pi \ : \quad U = \sum_{i=1}^{N} c_i U_i \in \mathbb{R}^{\mathfrak{M}} \mapsto U_{|H} = \sum_{i=1}^{N_H} c_i U_i^H \in \mathbb{R}^{\mathfrak{M}_H}. \tag{7}$$

Equivalently, Π can be seen as a simple truncation operation:

$$\Pi \ : \quad U = (c_i)_{1\leq i\leq N} \in \mathbb{R}^{\mathfrak{M}} \mapsto U_{|H} = (c_i)_{1\leq i\leq N_H} \in \mathbb{R}^{\mathfrak{M}_H},$$

following the above described identification between $\mathbb{R}^{\mathfrak{M}}$ and $\mathbb{R}^N$ and between $\mathbb{R}^{\mathfrak{M}_H}$ and $\mathbb{R}^{N_H}$. The transpose mapping ${}^T\Pi$ for Π reads:

$${}^T\Pi \ : \quad U = \sum_{i=1}^{N_H} c_i U_i^H \in \mathbb{R}^{\mathfrak{M}_H} \mapsto \sum_{i=1}^{N_H} c_i U_i \in \mathbb{R}^{\mathfrak{M}}.$$

We point out that in this discrete setting ${}^T\Pi$ does not match the prolongation by zero outside H. The following property will be useful:

$$\Pi\,{}^T\Pi = id_{\mathbb{R}^{\mathfrak{M}_H}}. \tag{8}$$

Let us introduce the mass matrices M, M_H and the stiffness matrices S_1, S_i so that:

$$\forall\ U_1, U_2 \in \mathbb{R}^{\mathfrak{M}}:\ \int_\Omega U_1U_2dx = (MU_1, U_2)_{\mathfrak{M}},\ \int_\Omega \overline{\sigma}_1\nabla U_1\cdot\nabla U_2dx = (S_1U_1, U_2)_{\mathfrak{M}}$$
$$\forall\ V_1, V_2 \in \mathbb{R}^{\mathfrak{M}_H}:\ \int_H V_1V_2dx = (M_HV_1, V_2)_{\mathfrak{M}_H},\ \int_H \sigma_i\nabla V_1\cdot\nabla V_2dx = (S_iV_1, V_2)_{\mathfrak{M}_H}$$

The second assumption on the space discretization reads:

($H2$) Let us denote I_Ω and I_H the characteristic functions of Ω and H respectively (constant functions equal to one):

$$I_\Omega \in \mathbb{R}^{\mathfrak{M}}\ ,\quad I_H \in \mathbb{R}^{\mathfrak{M}_H}. \tag{9}$$

Assumption ($H2$) is related with the considered boundary conditions here: homogeneous Neumann on $\partial\Omega$ and transmission conditions on ∂H. It implies that the stiffness matrices S_1, S_i (which are symmetric and non negative) have for kernels the one dimensional spaces $I_\Omega\mathbb{R}$ and $I_H\mathbb{R}$ respectively.

3.2. **Scheme statement.** The three unknowns v, u and $\mathbf{w}$ of the (continuous) bidomain model are represented by the discrete functions $U \in \mathbb{R}^{\mathfrak{M}}$, $V \in \mathbb{R}^{\mathfrak{M}_H}$ and $W \in [\mathbb{R}^{\mathfrak{M}_H}]^p$.
We have for $U \in \mathbb{R}^{\mathfrak{M}}$ and $V \in \mathbb{R}^{\mathfrak{M}_H}$:

$$\int_H \sigma_i\nabla V\cdot\nabla U dx = (S_iV, \Pi U)_{\mathfrak{M}_H} = ({}^T\Pi S_iV, U)_{\mathfrak{M}}$$

Discretization of (6) thus reads:

$$\begin{cases} S_1U^{n+1} + {}^T\Pi S_iV^{n+1} = 0, \\ \chi cM_H\dfrac{V^{n+1}-V^n}{\Delta t} + \chi M_H\left(I_{ion}(V^n, W^n) - I_{st}^n\right) = -S_i\Pi U^{n+1} - S_iV^{n+1} \end{cases}. \tag{10}$$

We introduce the positive parameter γ:

$$\gamma := \chi c/\Delta t.$$

Resolution algorithm. The complete bidomain model (1) (2) (3) is numerically solved applying the following three operations at each time step.
Being given $V^n \in \mathbb{R}^{\mathfrak{M}}$ and $W^n \in [\mathbb{R}^{\mathfrak{M}_H}]^p$:

Step 1. Compute the right hand side Y:

$$Y := \begin{bmatrix} 0 \\ M_H\left(\gamma V^n - \chi(I_{ion}(V^n, W^n) - I_{st}^n)\right) \end{bmatrix}.$$

Step 2. find the solution $X = {}^T[U^{n+1}, V^{n+1}]$ to $\Lambda X = Y$ with

$$\Lambda := \begin{bmatrix} S_1 & {}^T\Pi S_i \\ S_i\Pi & \gamma M_H + S_i \end{bmatrix} \quad \text{that satisfies} \quad \int_\Omega U^{n+1}dx = 0. \tag{11}$$

Step 3. Update the gating variable by computing W^{n+1} according to line 3 in equation (2).

□

This paper is devoted to Step 2 only. Proposition 1 states that step 2 is well posed.

4. Properties and LU factorization of the system matrix Λ

Let us precise that $S_1 : \mathbb{R}^{\mathfrak{M}} \mapsto \mathbb{R}^{\mathfrak{M}}$ and that $S_i : \mathbb{R}^{\mathfrak{M}_H} \mapsto \mathbb{R}^{\mathfrak{M}_H}$. Then, $\Lambda : \mathbb{R}^{\mathfrak{M}} \times \mathbb{R}^{\mathfrak{M}_H} \mapsto \mathbb{R}^{\mathfrak{M}} \times \mathbb{R}^{\mathfrak{M}_H}$.

Proposition 1. *The system matrix Λ is symmetric non negative with kernel $\mathrm{Ker}\,(\Lambda) = I_\Omega\mathbb{R} \times \{0\}$. By symmetry Λ has for range $\mathrm{Ran}\,(\Lambda) = I_\Omega^\perp \times \mathbb{R}^{\mathfrak{M}_H}$. For all $(Y_1, Y_2) \in I_\Omega^\perp \times \mathbb{R}^{\mathfrak{M}_H}$, there exists a unique $(U, V) \in \mathbb{R}^{\mathfrak{M}} \times \mathbb{R}^{\mathfrak{M}_H}$ such that*

$$\Lambda \begin{bmatrix} U \\ V \end{bmatrix} = \begin{bmatrix} Y_1 \\ Y_2 \end{bmatrix} \qquad \text{and} \quad \int_\Omega U dx = 0. \tag{12}$$

The resolution of step 2 in the resolution algorithm proceeds in two steps: first find a solution ${}^T[X_1, X_2]$, then normalize X_1. We now focus on the first step.

Definition 1 (Pseudo-inverses $\widetilde{S_1^{-1}}$ and $\widetilde{S_i^{-1}}$)**.** *The stiffness matrices S_1 and S_i are isomorphisms on $I_\Omega^\perp = \mathrm{Ran}\,(S_1)$ and on $I_H^\perp = \mathrm{Ran}\,(S_i)$ respectively. We introduce their pseudo inverse $\widetilde{S_1^{-1}}$ and $\widetilde{S_i^{-1}}$: they respectively are equal to the inverse of S_1, S_i on $I_\Omega^\perp$, $I_H^\perp$ and equal to 0 on $I_\Omega\mathbb{R}$, $I_H\mathbb{R}$.*
Considering p_Ω (resp p_H) the orthogonal projection of $\mathbb{R}^{\mathfrak{M}}$ on $I_\Omega^\perp$ (resp. of $\mathbb{R}^{\mathfrak{M}_H}$ on $I_H^\perp$). we have:

$$\widetilde{S_1^{-1}} S_1 = S_1 \widetilde{S_1^{-1}} = p_\Omega \ , \quad \widetilde{S_i^{-1}} S_i = S_i \widetilde{S_i^{-1}} = p_H \ .$$

Proposition 2. *We have the block decomposition $\Lambda = LU$ with:*

$$L := \begin{bmatrix} S_1 & 0 \\ S_i\Pi & K \end{bmatrix}, \quad U := \begin{bmatrix} id_{\mathbb{R}^{\mathfrak{M}}} & \widetilde{S_1^{-1}}\,{}^T\Pi S_i \\ 0 & id_{\mathbb{R}^{\mathfrak{M}_H}} \end{bmatrix}, \tag{13}$$

The matrix K is symmetric, positive definite. It reads:

$$K := \gamma M_H + S_i - S_i \Pi \widetilde{S_1^{-1}}\,{}^T\Pi S_i. \tag{14}$$

Remark 1 (About the matrix K)**.** *Let us consider the tensor*

$$\overline{\sigma}_e(x) = \begin{cases} \sigma_e(x), & x \in H \\ \sigma_T(x), & x \in T \end{cases},$$

and denote S_e the associated stiffness matrix. Since S_1 and S_e have the same range $I_\Omega^\perp$, one can define the pseudo-inverse $\widetilde{S_e^{-1}}$ for S_e with the same meaning as for S_1.
The matrix K in (14) can be rewritten as

$$K = \gamma M_H + \left(S_i^{-1} + \Pi S_e^{-1}\,{}^T\Pi\right)^{-1}.$$

where all inverses are pseudo-inverses. This equality is precisely stated and proven in the proof of proposition 2. It is interesting to notice that the second term appears as the "harmonic mean" between the stiffness matrices S_i and S_e. At the discrete level, this is a transposition of the "bidomain operator" as defined in [4] *that was introduced as the harmonic mean between two diffusion operators.*
From a practical point of view, K is non sparse but will never be computed explicitly, only approximated in order to get a preconditioner.

Proposition 3. *L has a pseudo inverse $\widetilde{L^{-1}}$ in the following sense:*

$$L\widetilde{L^{-1}} = \widetilde{L^{-1}}L = \begin{bmatrix} p_\Omega & 0 \\ 0 & id_{\mathbb{R}^{\mathfrak{M}_H}} \end{bmatrix},$$

U is invertible, U^{-1} and $\widetilde{L^{-1}}$ read:

$$L^{\widetilde{-1}} = \begin{bmatrix} S_1^{\widetilde{-1}} & 0 \\ -K^{-1}S_i\Pi S_1^{\widetilde{-1}} & K^{-1} \end{bmatrix}, \quad U^{-1} = \begin{bmatrix} id_{\mathbb{R}^{\mathfrak{M}}} & -S_1^{\widetilde{-1}}\,{}^T\Pi S_i \\ 0 & id_{\mathbb{R}^{\mathfrak{M}_H}} \end{bmatrix}. \tag{15}$$

For $Y \in \mathrm{Ran}\,(\Lambda)$, a solution to $\Lambda X = Y$ is provided by $X = U^{-1}\widetilde{L^{-1}}Y$.

Remark 2 (About the time discretization)**.** *Skipping to another time discretization scheme will basically imply two changes: the computation of the right hand side (Step 1 in the resolution algorithm above) and the definition of K. In general the global structure of the system matrix Λ (which is symmetric non negative) as well as the positivity of K will not be affected by considering different time discretization: this is for instance the case for the Cranck-Nicholson scheme or for operator splitting schemes (Strang formula e.g.).*
Consequently the resolution strategy presented in proposition 3 can be adapted to different time discretization schemes, as well as the preconditioning of K as pointed out in the following section.

Proof of proposition 1. For $X = {}^T(U,V) \in \mathbb{R}^{\mathfrak{M}} \times \mathbb{R}^{\mathfrak{M}_H}$, we have:

$${}^TX\Lambda X = (S_1U,U)_{\mathfrak{M}} + 2(S_i\Pi U,V)_{\mathfrak{M}_H} + (S_iV,V)_{\mathfrak{M}_H} + \gamma(M_HV,V)_{\mathfrak{M}_H}$$

We consider S_e and $\overline{\sigma}_e$ defined in Rem. 1. Since $\overline{\sigma}_1 - \overline{\sigma}_e$ is equal to 0 on T and to σ_i on H, $S_1 - S_e$ is non negative.

Equation (8) says that $\left({}^T\Pi V\right)_{|H} = \Pi\,{}^T\Pi V = V$. Together with $\overline{\sigma}_1 - \overline{\sigma}_e = 0$ outside H one gets:

$$\begin{aligned}
(S_iV,V)_{\mathfrak{M}_H} &= \int_H (\overline{\sigma}_1 - \overline{\sigma}_e)\nabla V \cdot V\; dx \\
&= \int_\Omega (\overline{\sigma}_1 - \overline{\sigma}_e)\nabla\,{}^T\Pi V \cdot \nabla\,{}^T\Pi V dx = \left((S_1 - S_e)\,{}^T\Pi V,\,{}^T\Pi V\right)_{\mathfrak{M}} \\
(S_i\Pi U,V)_{\mathfrak{M}_H} &= \int_H (\overline{\sigma}_1 - \overline{\sigma}_e)\nabla\Pi U \cdot \nabla V dx \\
&= \int_\Omega (\overline{\sigma}_1 - \overline{\sigma}_e)\nabla U \cdot \nabla\,{}^T\Pi V dx = \left((S_1 - S_e)U,\,{}^T\Pi V\right)_{\mathfrak{M}}.
\end{aligned}$$

From these two equalities we deduce that:

$${}^TX\Lambda X = (S_eU,U)_{\mathfrak{M}} + \left((S_1 - S_e)(U + {}^T\Pi V),(U + {}^T\Pi V)\right)_{\mathfrak{M}} + \gamma(M_HV,V)_{\mathfrak{M}_H}$$

so ensuring that Λ is non-negative. Assuming that $\Lambda X = 0$ implies that all the terms on the right of the last equality are equal to zero. The mass matrix being definite this means $V = 0$ and so $S_1U = 0$. Thus $U \in \mathrm{Ker}\,(S_1) = I_\Omega\mathbb{R}$ and we then have $\mathrm{Ker}\,(\Lambda) = I_\Omega\mathbb{R} \times \{0\}$.

Let $X = {}^T[U,V]$ be a solution to $\Lambda X = Y$ for $Y \in \mathrm{Ran}\,(\Lambda)$. A simple computation shows that $Z = {}^T[U - \alpha I_\Omega, V]$ is the unique solution to (12) iff $\alpha = (MU,I_\Omega)_{\mathfrak{M}}/(MI_\Omega,I_\Omega)_{\mathfrak{M}}$, so ending the proof. □

Proof of proposition 2. We have:

$$LU = \begin{bmatrix} S_1 & p_\Omega\, {}^T\Pi S_i \\ S_i\Pi & \gamma M_H + S_i \end{bmatrix},$$

and so $LU = \Lambda$ *iif* $p_\Omega\, {}^T\Pi S_i = {}^T\Pi S_i$. This last equality holds since for all $V \in \mathbb{R}^{\mathfrak{M}_H}$,

$$\left({}^T\Pi S_i V, I_\Omega\right)_\Omega = (S_i V, \Pi I_\Omega)_H = (S_i V, I_H)_H = 0,$$

and so $\mathrm{Ran}\left({}^T\Pi S_i\right) \subset I_\Omega^\perp$.

The symmetry of K is obvious. Let us prove it is positive definite.
We decompose $K = \gamma M_H + K_0$ so with $K_0 := S_i - S_i\Pi\widetilde{S_1^{-1}}\,{}^T\Pi S_i$. We will prove that K_0 (which is symmetric) is non negative. This implies the positivity of K since γM_H is positive definite. Precisely: K_0 clearly vanishes on $I_H\mathbb{R}$. Then $I_H^\perp$ is stable by K_0. Let us prove that K_0 is positive definite on $I_H^\perp$.

We consider again S_e and $\overline{\sigma}_e$ defined in Rem. 1. Let us first prove that:

$$K_0 = \Pi S_e \widetilde{S_1^{-1}}\,{}^T\Pi S_i \tag{16}$$

Firstly, we have: $\forall\ U_1.U_2 \in \mathbb{R}^{\mathfrak{M}}$,

$$\int_\Omega (\overline{\sigma}_1 - \overline{\sigma}_e)\nabla U_1 \cdot \nabla U_2 dx = \int_H \sigma_i \nabla U_1 \cdot \nabla U_2 dx,$$

and so ${}^T\Pi S_i\Pi = S_1 - S_e$.
Secondly, multiplying K_0 by $\Pi\,{}^T\Pi = id_{\mathbb{R}^{\mathfrak{m}_H}}$ on the left gives:

$$\begin{aligned} K_0 = \Pi\,{}^T\Pi K_0 &= S_i - \Pi\,{}^T\Pi S_i\Pi\widetilde{S_1^{-1}}\,{}^T\Pi S_i \\ &= S_i - \Pi(S_1 - S_e)\widetilde{S_1^{-1}}\,{}^T\Pi S_i \\ &= S_i - \Pi(p_\Omega - S_e\widetilde{S_1^{-1}})\,{}^T\Pi S_i \\ &= \Pi S_e\widetilde{S_1^{-1}}\,{}^T\Pi S_i + S_i - \Pi p_\Omega\,{}^T\Pi S_i. \end{aligned}$$

One already showed in this proof that $p_\Omega\, {}^T\Pi S_i = {}^T\Pi S_i$ ensuring that $\Pi p_\Omega\, {}^T\Pi S_i = S_i$. This gives us (16).

Clearly $\widetilde{S_e^{-1}}$ and $\widetilde{S_i^{-1}}$ are positive definite on $I_\Omega^\perp$ and $I_H^\perp$ respectively. We moreover have ${}^T\Pi(I_H^\perp) \subset I_\Omega^\perp$ since for all $V \in I_H^\perp$:

$$\left({}^T\Pi V, I_\Omega\right)_\Omega = (V, \Pi I_\Omega)_H = (V, I_H)_H = 0.$$

Then $\Pi\widetilde{S_e^{-1}}\,{}^T\Pi$ is positive definite on $I_H^\perp$. Let us define $A := (\widetilde{S_i^{-1}} + \Pi\widetilde{S_e^{-1}}\,{}^T\Pi)$: $I_H^\perp$ is stable by A. A is positive definite and so invertible on $I_H^\perp$. We will end this proof by showing that $K_0 = A^{-1}$ on $I_H^\perp$.

$$\begin{aligned} K_0 A &= (\Pi S_e\widetilde{S_1^{-1}}\,{}^T\Pi S_i)(\widetilde{S_i^{-1}} + \Pi\widetilde{S_e^{-1}}\,{}^T\Pi) \\ &= \Pi S_e\widetilde{S_1^{-1}}\,{}^T\Pi p_H + \Pi S_e\widetilde{S_1^{-1}}\,{}^T\Pi S_i\Pi\widetilde{S_e^{-1}}\,{}^T\Pi \\ &= \Pi S_e\widetilde{S_1^{-1}}\,{}^T\Pi p_H + \Pi S_e\widetilde{S_1^{-1}}(S_1 - S_e)\widetilde{S_e^{-1}}\,{}^T\Pi \\ &= \Pi S_e\widetilde{S_1^{-1}}\,{}^T\Pi p_H + \Pi S_e(p_\Omega\widetilde{S_e^{-1}} - \widetilde{S_i^{-1}}p_\Omega)\,{}^T\Pi \\ &= \Pi S_e\widetilde{S_1^{-1}}\,{}^T\Pi p_H + \Pi S_e(\widetilde{S_e^{-1}} - \widetilde{S_i^{-1}})\,{}^T\Pi \\ &= \Pi p_\Omega\,{}^T\Pi + \Pi S_e\widetilde{S_1^{-1}}\,{}^T\Pi(p_H - id_{\mathbb{R}^{\mathfrak{m}_H}}). \end{aligned}$$

Clearly, $p_H - id_{\mathbb{R}^{\mathfrak{m}_H}}$ vanishes on $I_H^\perp$. Moreover, since ${}^T\Pi(I_H^\perp) \subset I_\Omega^\perp$, $\Pi p_\Omega {}^T\Pi$ is the identity on $I_H^\perp$. Thus $K_0 AV = V$ for all $V \in I_H^\perp$. □

5. Preconditioning

5.1. Preconditioner definition.

Definition 2. *Let us consider P_1 a preconditioner for S_1 and P_K a preconditioner for K. We define a global preconditioner P_Λ for Λ as:*

$$P_\Lambda = L_P U_P \ , \quad L_P := \begin{bmatrix} P_1 & 0 \\ S_i\Pi & P_K \end{bmatrix}, \quad U_P := \begin{bmatrix} id_{\mathbb{R}^{\mathfrak{m}}} & P_1^{-1}\,{}^T\Pi S_i \\ 0 & id_{\mathbb{R}^{\mathfrak{m}_H}} \end{bmatrix}. \tag{17}$$

Preconditioning S_1 is a well documented operation (see e.g. [24] for the Preconditioning of diffusion operators).

The crucial point is the preconditioning of K. As already observed in Rem. 1, K has a complex structure:

$$K = \gamma M_H + K_0,$$

where K_0 is a non sparse matrix obtained by making the harmonic mean between S_i and S_e. Let us consider the tensor σ_m:

$$\sigma_m(x) := (\sigma_e^{-1}(x) + \sigma_i^{-1}(x))^{-1} \ , \quad x \in H,$$

which is the harmonic mean between σ_i and σ_e. We introduce the stiffness matrix S_m associated to σ_m acting on $\mathbb{R}^{\mathfrak{M}_H}$. We make the following approximation:

$$K \simeq K_m := \gamma M_H + S_m.$$

This approximation is referred to as the *monodomain model approximation* [9].
The matrix K_m has a simple structure. It reads the form of the discretization of a parabolic equation. It is moreover sparse (with the same pattern as S_i). The preconditioning of such a matrix also is well documented (see again [24]).

5.2. Practical details.

Let us start with the practical implementation of P_1 and P_K. As already stated: their definitions only involve the preconditioning of stiffness matrices. Efficient choices are for instance incomplete Cholesky or multigrid preconditioners. We refer to [24] for more details.
The numerical results below have been obtained within the framework of hierarchical matrices. This method allows to compute approximation for an elliptic matrix of a given accuracy (in matrix norm). The two basic steps to build this approximation are: (1) hierarchical construction of a block partition of the matrix, (2) blockwise approximation by low rank matrices. A Cholesky factorization of this approximation is here considered. This factorisation is stored into a data sparse format providing a low storage cost approxination of a full matrix (the $L^T L$ factorization of the original stiffness matrix). Using this factorised approximation as a preconditioner leads to an almost linear complexity (i.e. $n \log^\alpha(n)$, with n the matrix size) for tha matrix inversion. We refer to [3, 14, 15] for more details.
The preconditionners P_1 and P_K for S_1 and K are built in such a way using the H-Lib code from L. Grasedyck and S. Börm[1]. Their storage into a $L^T L$ sparse-format then make their inversion easy: these inversions have also been made using the H-Lib code.

[1] http://www.hlib.org/

The practical strategy to solve (11) will be to use an iterative solver to solve the left preconditioned system:

$$P_\Lambda^{-1}\Lambda X = P_\Lambda^{-1}Y.$$

The symmetry and positivity properties of Λ allow to adopt a Conjugate Gradient (CG) algorithm for this.

Let us point out the cost of our global preconditioner P_Λ. Each iteration of the CG algorithm involves a multiplication by Λ and an inversion of $P_\Lambda^{-1}X = Y$. In terms of storage these matrices do not need to be computed.
Three (sparse) matrices have to be stored for the multiplication by Λ: S_1, S_i and M_H. The operational cost for a multiplication by Λ is:

- 2 multiplications by S_i
- 1 multiplication by S_1
- 1 multiplication by M_H

To invert $P_\Lambda X = Y$, the two preconditioners P_1 and P_K also have to be stored. The inversion is achieved by computing $X = U_P^{-1}L_P^{-1}Y$ with:

$$L_P^{-1} := \begin{bmatrix} P_1^{-1} & 0 \\ -P_K^{-1}S_i\Pi P_1^{-1} & P_K^{-1} \end{bmatrix}, \quad U_P^{-1} := \begin{bmatrix} id_{\mathbb{R}^{\mathfrak{m}}} & -P_1^{-1}\,{}^T\Pi S_i \\ 0 & id_{\mathbb{R}^{\mathfrak{m}_H}} \end{bmatrix}. \tag{18}$$

The inversion has the following operational cost:

- 2 inversions of P_1,
- 1 inversion of P_K,
- 2 multiplications by S_i,

Globally, one CG iteration costs 6 matrix-vector multiplications and 3 preconditioner inversions. One adds that in the previous cost statements the vector addition as well as the multiplication by Π and ${}^T\Pi$ (which simply are vector truncation or prolongation by zero) have been neglected with regards to the matrix-vector multiplications and preconditioner inversions.

6. Numerical results

The efficiency of the preconditioner presented in Sec. 5 is analyzed in this section. The bidomain model has been implemented following Sec. 3 and using a finite volume spatial discretization (namely the CVFE scheme, see e.g. [5]). For this spatial discretization the degrees of freedom are located at the mesh vertices and the mass matrices are diagonal. Two test cases are considered: a two dimensional realistic setting and a three dimensional academical test presented below. For these two test cases a depolarization potential wave is simulated. This depolarization wave corresponds to the ventricular electrical excitation that precedes and induces its contraction, numerically it is by far the stiffest part of the simulation. We then compute and analyze the cost of the preconditioned system matrix inversion (11) during the spreading of the depolarization wave.

For both two test cases, we measured the average cost for one system matrix inversion (11) during the depolarization sequence. We then analyze the dependence of this cost with the problem size (the number of vertices or # Dof of the mesh here). The cost has been measured in two ways. Firstly in terms of CPU time. This method might however be perturbed by cacheing-effects and memory-access differences for large-scale problems. These perturbations are clearly visible for the largest 3D simulation where more that 11 Gos of memory were involved. For this reason we

	Values	Unit
Cell membrane surface-to-volume ratio (2D)	$\chi = 1500$	$[\text{cm}^{-1}]$
Cell membrane surface-to-volume ratio (3D)	$\chi = 500$	”
Membrane surface capacitance	$c = 1.$	$[\mu\ \text{F/cm}^2]$
Longitudinal intra-cellular conductivity	$g_i^l = 1.741$	[mS/cm]
Transverse intra-cellular conductivity	$g_i^t = 0.1934$	”
Longitudinal extra-cellular conductivity	$g_e^l = 3.906$	”
Transverse extra-cellular conductivity	$g_e^t = 1.970$	”
Lung conductivity	0.5	”
Blood conductivity (ventricle cavities)	6.7	”
Remaining tissues conductivity	2.2	”

TABLE 1. Model parameters

also measured the average number of iterations required per system inversion. The cost then is defined as the average number of iterations required times the problem size.

6.1. **Test cases.** For the two test cases, the reaction terms $I_{ion}(v, \mathbf{w})$ and $g(v, \mathbf{w})$ in (2) have been set to the Luo and Rudy ionic model of class II [18] designed for mammalian ventricular cells and for which the system of ODEs in (2) is of size 20 (i.e. $\mathbf{w} \in \mathbb{R}^{20}$). The model parameters χ, c as well as the conductivities are displayed in Tab.1: these values are physiological values taken from [17, 26].

2D test case. The domain Ω is an horizontal slice of a human thorax. This geometry has been obtained by segmenting a medical image (CT-Scan, courtesy of the Ottawa Heart Institute) with resolution 0.5 mm. We refer to [22, 23] for details on the segmentation procedure. The segmented image is depicted in Fig. 1. It includes 4 sub domains: the two ventricles (H), the ventricular cavities, the lungs and the remaining tissues (T). Four meshes of Ω will be considered: roughly from 145 000 to 1 250 000 vertices (see Tab. 2 for exact figures). The anisotropic structure of the two ventricles is displayed on Fig1: bundles of fibres rotating around the ventricular cavities have been considered. Inside the torso T, heterogeneous conductivities have been considered for each sub domains: the lungs, ventricular cavities and the remaining tissues conductivities are given in Tab. 1.

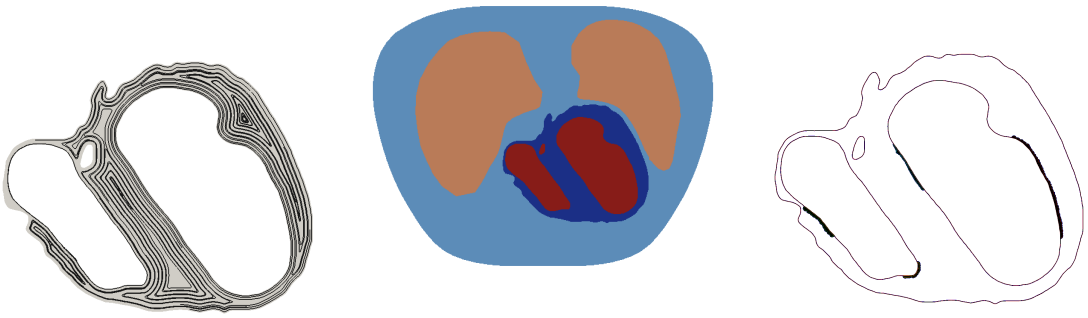

FIGURE 1. 2D test case description. Left: fibrous anisotropic structure of the two ventricles. Middle: 2D geometry Ω and its sub domains. Right: stimulation site locations.

With these settings, a depolarization potential wave is simulated. For this a stimulation current $I_{st}(x,t)$ (see equation (2)) is applied during one ms at four locations (stimulation sites) on the ventricle cavities as depicted on Fig. 1. The spreading of this potential wave across the myocardium is depicted on Fig. 2. Without entering the details: the region in blue is at rest potential ($v \simeq -90$ mV) whereas the region in red is excited ($v \simeq -30$ mV). The excitation starts at the stimulation site location and then spreads throughout the cardiac tissue (from the left to the right).

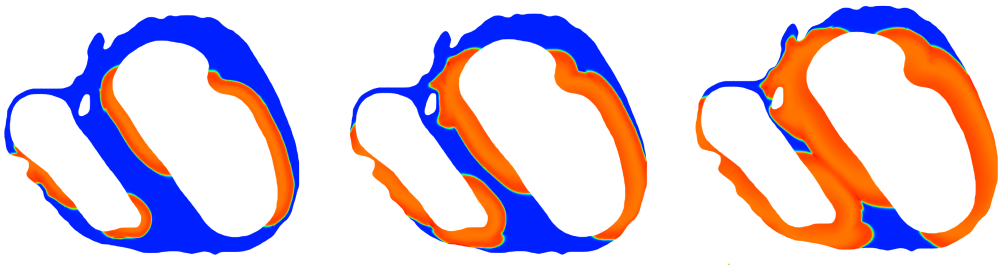

FIGURE 2. 2D case: propagation of the depolarization wave across the cardiac tissues.

3D test case. We consider an academical test case where the geometry is the unit cube $[0,1]^3$. A series of 5 meshes has been considered, from 500 to 1 250 000 vertices (see Tab. 2 for exact figures). The heart is here considered as isolated: no torso T is involved as described in Sec. 2.2. The cardiac tissue is still considered as anisotropic but the muscular fibres are supposed to have a constant direction along the x-axis (constant anisotropy).
A depolarization potential wave is simulated by applying a stimulation current at the centre of the domain.

#DOF	Average #iterations
143 053	17.6
344 408	22.2
684 112	25.3
1 257 312	26.8

(a) 2D case

# DOF	Average # iterations
497	9.26
3 220	10.93
22 256	11.15
162 981	11.52
1 253 910	11.56

(b) 3D case

TABLE 2. Average number of iterations for one system inversion.

6.2. **Results.** For the 2D case, the cost is depicted on Fig. 3 (on the left). The cost is represented in function of the problem size in log / log scale. In term of CPU time (above) the data fit a linear mapping of slope 1.0 (using a least square approximation). The linear progression between two successive data points being bounded between 1.03 and 0.93. Considering the cost in terms of average number of iterations, the data globally fit a linear mapping of slope 1.21. However, the linear progression rate between two successive data points decreases from 1.29 to 1.09. The average number of iterations needed per inversion is given in Tab. 2.

For the 3D case, the cost in term of CPU time did not provide satisfactory results for the large scale simulations. The cost in term of the average number of iterations

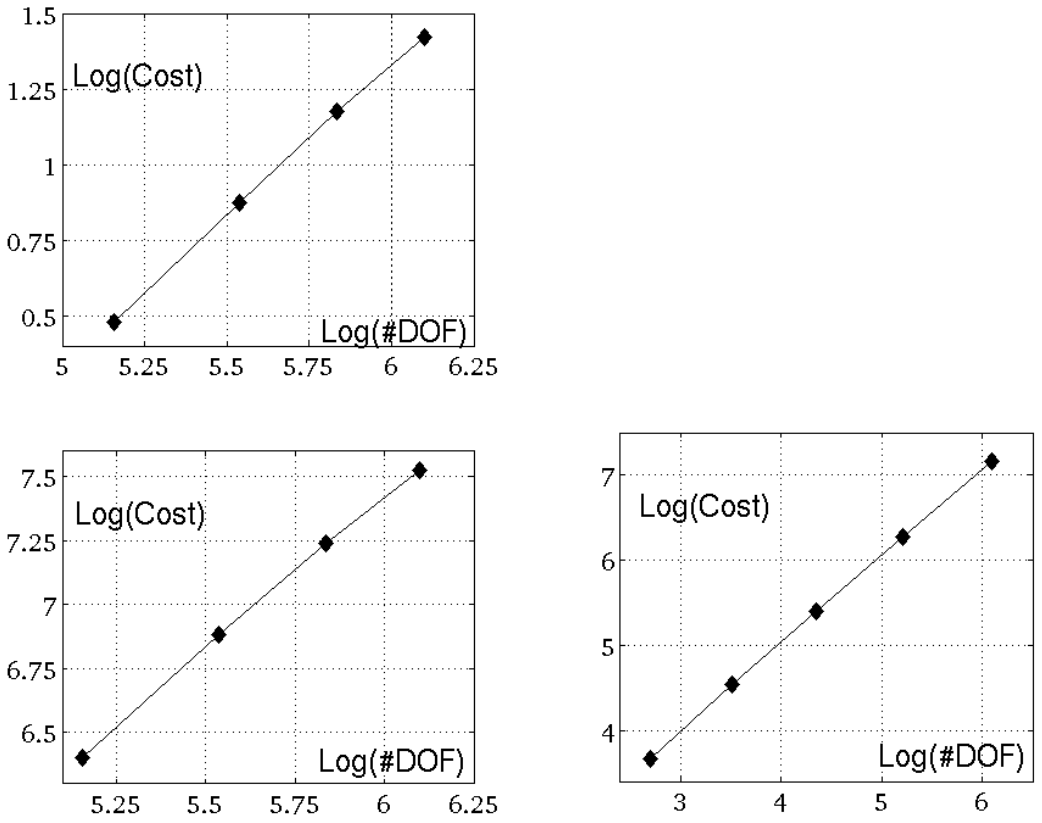

(a) 2D case (b) 3D case

FIGURE 3. Cost of one inversion of $\Lambda X = Y$ as a function of the problem size in Log/Log scale. Above: the cost is measured in terms of CPU time consumption (2D case only). Below: the cost is relative to the average number of iterations needed.

is given in Tab. 2 (on the right) and depicted on Fig. 3 (also on the right). The cost is again represented in function of the problem size in log / log scale. The data fit with a straight line of slope 1.03. The linear progression between two successive data points being bounded between 1.09 and 1.00.

For both test cases, we numerically observed an almost linear dependence of the system matrix inversion cost with the problem size. From these observations it seems reasonable to conclude to an almost linear complexity (of type $n \log^{\alpha}(n)$): this conclusion being in agreement with theoretical results, the hierarchical matrix preconditioning for elliptic problems providing such a complexity [14].

However, let us point out that even assuming a linear dependence for the cost with respect to the number of nodes, this still implies an h^{-d} dependence of the cost with the mesh size h and with d the dimension. Considering the global cost of the simulation and not only the cost of one inversion, this now leads to an $h^{-(d+1)}$ dependence of the cost with the mesh size. Thus a linear dependence of one system inversion cost with respect to the problem size still leads to really heavy global costs for this type of problems.

References

[1] L. Ambrosio, P. Colli-Franzone, and G. Savaré. On the asymptotic behaviour of anisotropic energies arising in the cardiac bidomain model. *Interfaces Free Bound.*, 2(3):213–266, 2000.

[2] B. Andreianov, M. Bendahmane, K. H.. Karlsen, and C. Pierre. Convergence of DDFV schemes for the bidomain cardiac model. *HAL Preprint*, 2010.

[3] S. Boerm, L. Grasedyck, and W. Hackbusch. An introduction to hierarchical matrices with applications. *Eng. Anal. Bound.*, 27:405–422, 2003.

[4] Y. Bourgault, Y. Coudière, and C. Pierre. Existence and uniqueness of the solution for the bidomain model used in cardiac electrophysiology. *Nonlinear Analysis: Real World Applications*, 10(1):458–482, 2009.

[5] Z. Cai, J. Mandel, and S. McCormick. The finite volume element method for diffusion equations on general triangulations. *SIAM J. Numer. Anal.*, 28:392–403, 1991.

[6] J.C. Clements, J. Nenonen, P K. Li, and M. Horácek. Activation dynamics in anisotropic cardiac tissue via decoupling. *Annals Biomed. Eng.*, 32(7):984–990, 2004.

[7] P. Colli Franzone, P. Deuflhard, B. Erdmann, J. Lang, and L. F. Pavarino. Adaptivity in space and time for reaction-diffusion systems in electrocardiology. *SIAM J. Sci. Comput.*, 28(3):942–962 (electronic), 2006.

[8] P. Colli Franzone and L.F. Pavarino. A parallel solver for reaction-diffusion systems in computational electrocardiology. *Math. Models Methods Appl. Sci.*, 14(6):883–911, 2004.

[9] P. Colli-Franzone, L.F. Pavarino, and B. Taccardi. Simulating patterns of excitation, repolarization and action potential duration with cardiac Bidomain and Monodomain models. *Math. Biosci.*, 197(1):35–66, 2005.

[10] P. Colli-Franzone and G. Savaré. Degenerate evolution systems modeling the cardiac electric field at micro- and macroscopic level. *Evolution equations, semigroups and functional analysis*, 2002.

[11] M. Ethier and Y. Bourgault. Semi-implicit time discretization schemes for the bidomain model. *SIAM Journal of Numerical Analysis*, 46(5):2443–2468, 2008.

[12] L. Gerardo-Giorda, L. Mirabella, F. Nobile, M. Perego, and A. Veneziani. A model-based block-triangular preconditioner for the bidomain system in electrocardiology. *J. Comput. Phys.*, 228(10):3625–3639, 2009.

[13] L. Gerardo-Giorda, M. Perego, and A. Veneziani. Optimized schwarz coupling of bidomain and monodomain models in electrocardiology. *M2AN*, 2010.

[14] L. Grasedyck and W. Hackbusch. Construction and arithmetics of $\mathcal{H}$-matrices. *Computing*, 70(4):295–334, 2003.

[15] L. Grasedyck, R. Kriemann, and S. Le Borne. Parallel black box $\mathcal{H}$-LU preconditioning for elliptic boundary value problems. *Comput. Vis. Sci.*, 11(4-6):273–291, 2008.

[16] W. Krassowska and J.C. Neu. Homogenization of syncytial tissues. *CRC Crit. Rev. Biomed. Eng.*, 21(2):137–199, 1993.

[17] P. Le Guyader, F. Trelles, and P. Savard. Extracellular measurement of anisotropic bidomain myocardial conductivities. I. theoretical analysis. *Annals Biomed. Eng.*, 29(10):862–877, 2001.

[18] C.H. Luo and Y. Rudy. A Dynamic Model of the Cardiac Ventricular Action Potential I. Simulations of Ionic Currents and Concentration Changes. *Circ. Res.*, 74:1071–1096, 1994.

[19] B.F. Nielsen, T.S. Ruud, G.T. Lines, and A. Tveito. Optimal monodomain approximations of the bidomain equations. *Applied Mathematics and Computation*, 184:276–290, 2007.

[20] C. Pierre and Y. Bourgault. A comparison of the Bidomain and the adapted monodomain models in electro-cardiology. *HAL Preprint*, 2010.

[21] M. Potse, B. Dube, J. Richer, A. Vinet, and RM. Gulrajani. A comparison of monodomain and bidomain reaction-diffusion models for action potential propagation in the human heart. *IEEE Trans. Biomed. Eng.*, 53(12):2425–2435, 2006.

[22] O. Rousseau. Geometrical modeling of the heart. *PHD Thesis, University of Ottawa*, 2010.

[23] O. Rousseau and Y. Bourgault. Heart segmentation with an iterative Chan-Vese algorithm. *HAL Preprint*, 2009.

[24] Y. Saad. *Iterative methods for sparse linear systems*. Society for Industrial and Applied Mathematics, Philadelphia, PA, second edition, 2003.

[25] S. Sanfelici. Convergence of the galerkin approximation of a degenerate evolution problem in electrocardiology. *Numer. Methods for Partial Differential Equations*, 18:218–240, 2002.
[26] N.P. Smith, M.L. Buist, and A.J. Pullan. Altered t wave dynamics in contracting cardiac model. *J. Cardiovascular Electrophysio.*, 14:5203–5209, 2003.
[27] J. Sundnes, B.F. Nielsen, K.A. Mardal, X. Cai, G.T. Lines, and A. Tveito. On the computational complexity of the bidomain and the monodomain models of electrophysiology. *Annals of Biomedical Engineering*, 34:1088–1097, 2006.
[28] L. Tung. A bidomain model for describing ischemic myocardial D-D properties. *Ph.D. thesis, M.I.T..*, 1978.
[29] M. Veneroni. Reaction-diffusion systems for the microscopic cellular model of the cardiac electric field. *Math. Methods Appl. Sci.*, 29(14):1631–1661, 2006.

(Charles Pierre)
Laboratoire de Mathématiques et Applications
Université de Pau et du Pays de l'Adour
av. de l'Université BP 1155
64013 PAU Cedex - FRANCE
E-mail address: charles.pierre@univ-pau.fr